Chin. Sci. Bull. (2014) 59(14):1508–1518
DOI 10.1007/s11434-014-0232-7

csb.scichina.com
www.springer.com/scp

Article

Atmospheric Science

Methane retrieval from Atmospheric Infrared Sounder using EOF-based regression algorithm and its validation

Ying Zhang · Xiaozhen Xiong · Jinhua Tao · Chao Yu · Mingmin Zou · Lin Su · Liangfu Chen

Received: 1 July 2013 / Accepted: 20 November 2013 / Published online: 15 April 2014

Abstract This paper presents a rapid regression algorithm for the retrieval of methane (CH_4) profile from Atmospheric Infrared Sounder (AIRS) based on empirical orthogonal functions (EOF) and its validation. This algorithm was trained using the simulated radiance from an assemble of atmospheric profiles and can be utilized to derive the CH_4 profile rapidly with the input of the AIRS cloud-clear radiance. Validation using hundreds of aircraft profiles demonstrates that the root mean square error (RMSE) is about 1.5 % in the AIRS sensitive region of 359–596 hPa, which is smaller than AIRS-V5 product (except in high latitudes). Comparison with the ground-based solar Fourier transform spectrometry observations showed that the RMSE of the retrieved CH_4 total column amount is less than 3 %. This EOF-based regression method can be easily applied to other thermal infrared sounders for deriving CH_4 and some other gases, and the derived profiles can be used as the first guess for further physical retrieval.

Keywords EOF · Methane · AIRS · Remote sensing · Regression

SPECIAL TOPIC Greenhouse Gas Observation From Space: Theory and Application

Y. Zhang · J. Tao · C. Yu · M. Zou · L. Su · L. Chen (✉)
State Key Laboratory of Remote Sensing Science, Institute of Remote Sensing and Digital Earth, Chinese Academy of Sciences, Beijing 100101, China
e-mail: lfchen@irsa.ac.cn

X. Xiong
NOAA Center for Satellite Applications and Research, College Park, MD 20740, USA

1 Introduction

Following water vapor and carbon dioxide (CO_2), methane (CH_4) is the most abundant greenhouse gas in the troposphere. The abundance of CH_4 is about 1,774 ppbv (volume parts per billion) in 2005, much smaller than that of CO_2 (379 ppmv, volume parts per million), directly contributing 0.48 W m^{-2} to the total anthropogenic radiative forcing of 2.63 W m^{-2} by well-mixed greenhouse gases [1]. However, on both molecule and mass basis, CH_4 is much more effective than CO_2 in absorbing long-wave radiation, since its radiative forcing (RF) is 3.7×10^{-4} W m^{-2} ppb^{-1} compared to 1.4×10^{-5} W m^{-2} ppb^{-1} for CO_2. It also plays an important role in both tropospheric and stratospheric chemistry [1]. For example, the oxidation of CH_4 by hydroxyl (OH) in the troposphere leads to the formation of formaldehyde (CH_2O), carbon monoxide (CO), and ozone (O_3), in the presence of sufficiently high levels of nitrogen oxides (NO_x). Along with CO, CH_4 affects the amount of OH in the troposphere. Additionally, it affects the concentrations of water vapor and ozone in the stratosphere and also plays a key role in the conversion of reactive chlorine to less reactive HCl in the stratosphere [2].

Current CH_4 concentrations are about 2.5 times higher than those of the pre-industrial atmosphere [3]. This increase is presumably driven by increasing emissions, but may also reflect changes in the chemical sink (reaction with the OH radical) [1]. From 1999 to 2006, globally averaged CH_4 was relatively constant. The increase in its growth rate since 2007–2009 raises concerns about the release of CH_4 from the thawing permafrost, as it has the potential to release a large amount of carbon to the atmosphere [4–6]. However, analysis of $\delta^{13}C$ CH_4 suggested the increase in 2007 and afterward was mainly driven by the increase tropical precipitation and a warmer summer in Arctic [5,

7]. The renewed CH_4 increase from mid 2006 to September 2011 has also been observed by ground-based solar Fourier transform spectrometry (FTS) at Zugspitze and Garmisch [8].

High-precision in situ measurements of CH_4 mixing ratios have been made at the networks of NOAA/ESRL/GMD (National Oceanic and Atmospheric Administration, Earth System Research Laboratory, Global Monitoring Division) and some other sites. It is possible to well quantify the global CH_4 budget of source and sink based on these in situ measurements and inverse modeling [9]. However, the quantification of different emission source types and source regions still has large uncertainties [10], owing to a large spatial and temporal variation of CH_4 emissions and limited sparse sites in ground observational network [11].

Recent developments of satellite observations enable us to measure the atmospheric CH_4 with a global coverage. One type of satellite observation of CH_4 is based on solar backscattered radiance in the near infrared (NIR) band, which is sensitive to the CH_4 in lower troposphere and its total column. However, it relies on the reflected sunlight and thus performs well only in cloud-free daytime and over land conditions. In addition, the NIR CH_4 retrieval accuracy strongly depends on aerosol as it impacts the NIR photon path in the atmosphere, a part that is hard to estimate [12]. Most recent column-average CH_4 (XCH_4) data from NIR observations can be accessed from Scanning Imaging Absorption SpectroMeter for Atmospheric CHartographY (SCIAMACHY) onboard ENVISAT for 2003–2009 [13] and from the Thermal and Near-infrared Sensor for carbon Observation (TANSO) on board Greenhouse gases Observing SATellite (GOSAT) since 2009 [14]. Validations of SCIAMACHY and GOSAT XCH_4 have been made using coincident observations from ground based FTS in a limited number of sites, mostly in Europe and eastern North America. The accuracy for GOSAT SWIR XCH_4 is 1.2 % ± 1.1 % [15], and for SCIAMACHY, it is 30 ppbv before November 2005 and 70 ppbv afterwards [16]. However, a precision of 1 %–2 % and an accuracy of at least 1 % are required for the use of CH_4 column amount from space-borne observations in the inverse modeling to derive CH_4 sources accurately [17].

Another type of space-borne observation of CH_4 is from thermal infrared sounder (TIR), which provides a better global coverage and works day and night (even for partial cloudy scenes). However, the peak sensitivity of TIR sounder is in the mid-upper troposphere and has limited sensitivity to the lower troposphere. The Interferometric Monitor of Greenhouse gases (IMG) aboard the Japanese Advanced Earth Observing Satellite (ADEOS) was the first space-borne instrument used to retrieve tropospheric CH_4 from the TIR [18], but with limited operational time from August 1996 to June 1997. The Tropospheric Emission Spectrometer (TES) aboard the EOS/Aura and the Infrared Atmospheric Sounding Interferometer (IASI) onboard European polar Meteorological Operational Platform (METOP-1) have provided TIR CH_4 retrievals since 2004 and 2007 [19–21], and the CH_4 retrievals have been validated, respectively [22–24]. As a stable space-borne thermal infrared sounder in operation, AIRS was launched on 4 May 2002 and has provided the longest CH_4 observation so far [25–27]. CH_4 retrieval from TIR/GOSAT is also available now [14].

The CH_4 retrievals from these NIR or TIR sensors are derived using different physical retrieval algorithms, and their first-guess profiles are either from model simulation or from climatology data. Since a good first-guess profile (*a priori*) and/or covariance matrices are essential to improve the accuracy and efficiency of physical retrievals from NIR or TIR observations regardless of the type of physical retrieval algorithms, and the CH_4 retrievals from TIR rely on the knowledge of water vapor and temperature profiles, which are either retrieved in advance [25] or retrieved simultaneously, a stable, rapid regression retrieval method based on empirical orthogonal function (EOF) are developed to retrieve CH_4 vertical profile using AIRS radiances only by Zhang et al. [28]. This method does not need a first guess and the information of water vapor and temperature profiles, and is much faster than physical retrievals, in which the computation of Jacobian matrices is time-consuming. This paper presented the improvement on this method, including re-selecting channels for retrieval, using cross validation to cut down the number of eigenvectors to avoid overfitting, and its validation using aircraft measurements of profiles and the ground-based measurements of total column amount. For comparison, the AIRS-V5 CH_4 product is also compared.

2 AIRS instrument and the regression algorithm based on EOF

As a stable space-borne thermal infrared sounder in operation, AIRS on NASA/EOS crosses the equator at approximately 1:30 a.m. and 1:30 p.m. (local time), resulting in near global coverage twice a day. AIRS has 2,378 channels covering from 649 to 1136, 1,217 to 1,613, and 2,169 to 2,674 cm^{-1} at high spectral resolution ($\lambda/\Delta\lambda = 1{,}200$). The noise equivalent change in temperature (NEDT) referred to a 250 K target temperature, ranging from 0.14 K in the critical 4.2 μm lower tropospheric sounding channels to 0.35 K in the 15 μm upper tropospheric sounding region. AIRS has a field of view (FOV) of 1.1°, corresponding to a nadir footprint of 13.5 km on the surface, and large scan angles between ±48.95°.

Atmospheric retrievals are performed in conjunction with Aqua's Advanced Microwave Sounding Unit (AMSU) at the AMSU spatial resolution of 45 km at nadir [29]. AIRS' channels cover the 4.2 and 15 μm CO_2 bands, 6.3 μm water vapor broadband, 9.6 μm ozone band, as well as the absorption bands of trace gases such as CH_4, N_2O, CO, and SO_2. Validations of AIRS-V5 CH_4 by Xiong et al. [25, 26] using thousands of aircraft profiles demonstrated that its root mean square error (RMSE) is mostly less than 1.5 %. Zhang et al. [30] validated AIRS CH_4 product with FTS retrieval at the National Satellite Meteorological Center in Beijing for 6 months in 2009, and obtained the similar result. Plume-like enhancement of CH_4 in the middle to upper troposphere over South Asia was observed during the monsoon season using AIRS [31] and its existence was further confirmed by aircraft measurements [32] and IASI observations [21].

An eigenvector regression algorithm (or principal component regression) provides a computationally efficient retrieval of atmospheric temperature, moisture, ozone, and surface skin temperature and emissivity [33]. In principle, a similar regression retrieval method could be developed for CH_4 retrieval likewise. However, due to the lack of in situ observation of CH_4 profiles (as truth), data of the simulated AIRS radiances corresponding to different CH_4 profiles were used to develop the EOF-based regression algorithm. In this paper, 80 atmospheric profiles from European Centre for Medium-Range Weather Forecasts (ECMWF) were used, and the radiances received by AIRS were simulated by RTTOV9.3 [34], a fast radiative transfer model incorporating the AIRS spectral response function and developed by ECMWF. The 80 profiles cover most regions worldwide from 75°N to 75°S in all seasons. In order to reduce the error induced by sun-viewing geometry, the simulated AIRS radiances were calculated at different viewing and incident zenith angles from 0° to 70° in an interval of 5°. Errors equivalent to the noise of AIRS were added to the simulated radiances randomly.

To develop the EOF-based regression algorithm in this paper, we derived the eigenvectors from the covariance matrices of the simulated radiances and the CH_4 mixing ratio profiles, and then obtained the coefficient matrix to transform the radiances to CH_4 mixing ratio profiles in their truncated EOF spaces. Once the coefficient matrix was available, the CH_4 profiles could be derived from the AIRS radiance observations directly. A more detailed description of this algorithm is found in Zhang et al. [28]. The cloud-cleared radiances from AIRS-V5 product (http://mirador.gsfc.nasa.gov/) are used in implementation.

To select the channels in the final retrieval, the corresponding variations of brightness temperature received by AIRS, averaged over the atmospheric profiles in training dataset, are computed for a variation of 10 % for CH_4, 10 % for H_2O, and 10 % for CO_2. And five sets of channel combinations were selected and compared. The pre-selected channel sets are listed in Table 1. All unstable and noisy channels (whose NEDT is greater than 0.2 K, including 388 of 2,378 channels) of AIRS were excluded from our channel lists.

Table 1 Pre-selected channel sets (388 noisy AIRS channels excluded)

Set	Wavenumber range (cm^{-1})	Number of channels	Comments
1	687–2,700	1,990	All channels whose NEDT is less than 0.2 K
2	1,217–1,382	164	The 7.7 μm CH_4 band, whose variation of brightness temperature is greater than 0.1 K for a variation of 10 % of CH_4
3	687–1613.9	675	including the 7.7 μm CH_4 band, the 15 μm CO_2 band and the 6.3 μm water vapor band, whose variation of brightness temperature is greater than 0.1 K for a variation of 10 % of CH_4, or 0.4 K for a variation of 10 % of H_2O, or 0.6 K for a variation of 10 % of CO_2
4	1,217–2,700	554	including the 7.7 μm CH_4 band, the 4.3 μm CO_2 band and the 6.3 μm water vapor band, and the criterion is the same as in set 3
5	687–2,700	1,826	all channels except the 7.7 μm CH_4 band

When all the profile samples were used for training and tested on the same samples, the smallest error was found by using channel set 2 with the first 78 eigenvectors in the radiance space and 50 eigenvectors in the profile space. This indicates that the 7.7 μm CH_4 band could provide sufficient information about CH_4, and that the addition of many other channels covering temperature and water vapor bands will induce redundancy, which reduces the accuracy and stability of the CH_4 retrieval. The error becomes larger if too many eigenvectors in the radiance space are used because the inverse of the matrix in coefficients expression will be unstable.

Since all the samples are used for training and none is left as independent test set, the EOF model is probably overfitted. Thus, we further used the leave-one-out cross-validation (LOOCV) to select the number of eigenvectors in the radiance space. The LOOCV involves using a single observation from the original samples as the validation data and the remaining observations as the training data. This process was repeated, thus each observation in the samples

was used once as the validation data. We found that it was easier to compare the RMSEs in the CH_4 total column amount than in the CH_4 profile in this process. Based on the RMSEs of the total column amount in the process of LOOCV corresponding to different channel sets and the number of eigenvectors in the radiance space (Fig. 1), we found the RMSE of channel set 2 can be further reduced using the first 40 eigenvectors in the radiance space. Finally, 164 channels in the 7.7 μm CH_4 absorption band (set 2), 40 eigenvectors in the radiance space, and 50 eigenvectors in the profile space were selected to build the regression retrieval algorithm in this paper.

The main interfering factor in CH_4 retrieval is H_2O, which dominates the infrared spectrum in the 7.7 μm CH_4 absorption bands. To examine whether this EOF model was sensitive to H_2O, the AIRS radiances were re-computed by shifting the H_2O profiles by 10 % (both plus and minus), and then were used to retrieve the CH_4 profiles. The result shows that the RMSEs of the retrieved CH_4 were nearly the same as before (Fig. 2), suggesting that the use of eigenvectors reduces the influences of random measurement errors and thus minimizes its sensitivity to H_2O error in this EOF-based regression model.

3 Validation

3.1 Profile comparison with in situ aircraft measurements

In situ aircraft measurements of CH_4 profiles are used for validations, which include the profiles from several campaigns, such as HIAPER Pole-to-Pole Observations (HIPPO) of Carbon Cycle and Greenhouse Gases Study [35], the Intercontinental Chemical Transport Experiment (INTEX)-A [36] and -B [37], Stratosphere–Troposphere Analyses of Regional Transport in 2008 (START08) [38], and The Arctic Research of the Composition of the Troposphere from Aircraft and Satellites (ARCTAS) [39]. The flight paths for these campaigns are shown in Fig. 3. Except for HIPPO, other campaigns focus on the Northern Hemisphere, especially North America, North Pacific Ocean, and Arctic. A brief description of the time of these campaigns and the number of profiles used is listed in Table 2.

The profiles from aircraft measurements in these seven campaigns are used as the truth for CH_4 validation. Corresponding to each aircraft profile, all AIRS retrieved profiles in a collocation window within ±24 h and ±200 km are used to compute their mean profile for comparison. The radiances are from AIRS Level-2 Version 5 Cloud-Cleared IR Radiance and only pixels with overall quality flags 1 are used. For comparison, the AIRS-V5 CH_4 profiles from AIRS Level-2 Version 5 support products in 100 layers are also used. They are both downloaded from http://mirador.gsfc.nasa.gov/.

Comparison in the AIRS layers from 200 to 845 hPa for seven campaigns was made. Since the top altitudes measured in different flights are different, the number of measurements in upper levels is less. Figure 4 shows the correlation coefficients between the aircraft measurements with the retrieved CH_4 from the EOF method and AIRS-V5, and Fig. 5 presents their RMSEs of the retrieved CH_4. The overall correlation coefficients (using all samples from seven campaigns) of CH_4 retrieved from the EOF method and AIRS-V5 with the aircraft measurements, as shown in

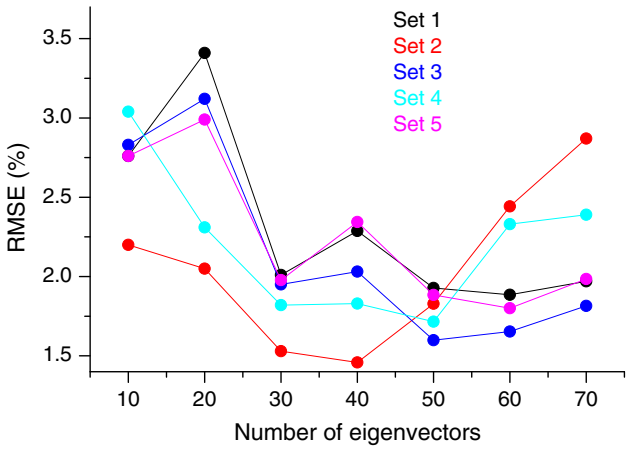

Fig. 1 The RMSEs of CH_4 total column amount for different numbers of eigenvectors in the radiance space and different channel sets using the LOOCV over the ECMWF atmospheric profiles. The minimum error occurs when using channel set 2 and 40 eigenvectors in the radiance space

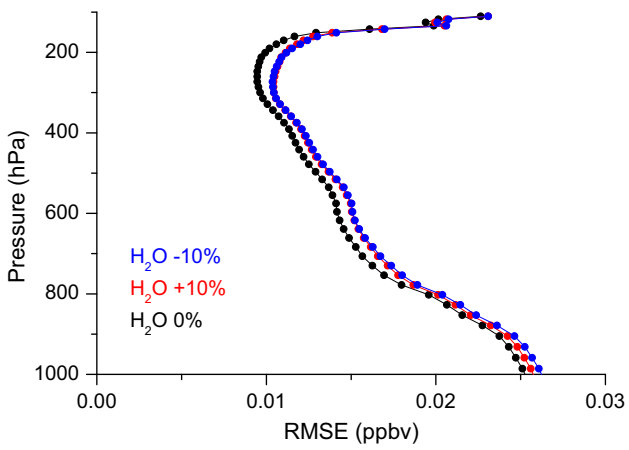

Fig. 2 (Color online) The RMSEs of CH_4 profiles retrieved from simulated radiances with the original coefficients. The *blue line* is the RMSE of CH_4 retrieved from radiances when H_2O profiles are shifted 10 % upper while the *red line* is that retrieved from radiances when H_2O profiles are shifted 10 % lower

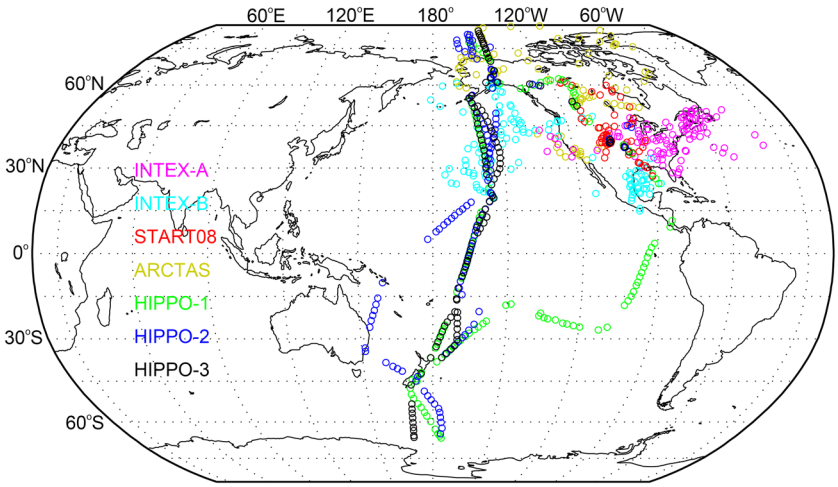

Fig. 3 The flight paths of INTEX-A, INTEX-B, START08, ARCTAS, HIPPO-1, HIPPO-2, and HIPPO-3, respectively

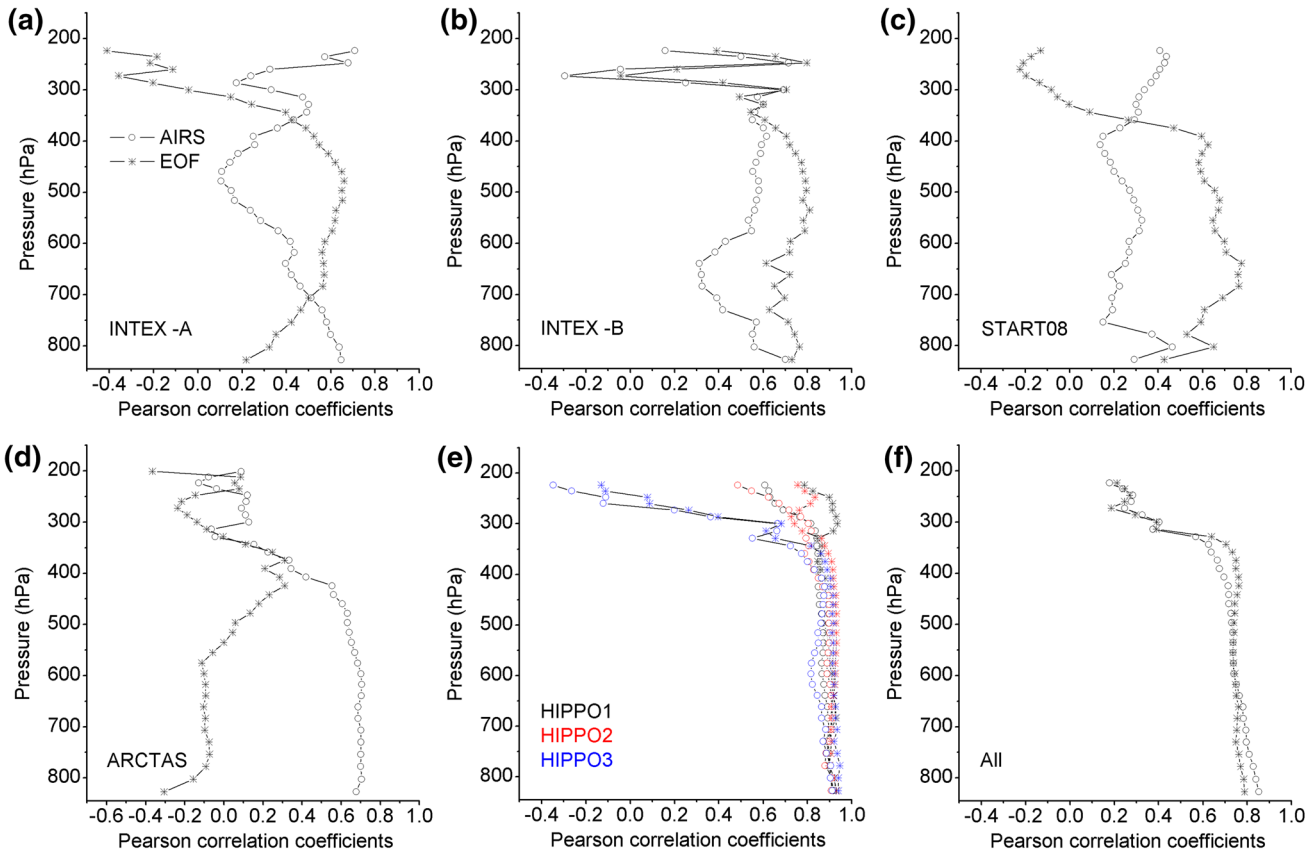

Fig. 4 The Pearson correlation coefficient (R) of CH_4 retrievals for seven campaigns. The *hollow circles* are AIRS V5.0 CH_4 product and stars are CH_4 retrieved from EOF method

Fig. 4f, are both close to 0.8, which means the CH_4 retrieved from AIRS data could describe the CH_4 trend to some extent. The correlation coefficients for HIPPO-1, -2, -3 for both AIRS-V5 and the EOF regression method are much larger than other four campaigns, which is mainly because HIPPOs cover a large latitudinal range from south to north, thus has a large variation in CH_4. The correlation coefficients of EOF retrievals are much smaller than AIRS-

Table 2 A brief description of 7 campaigns used for validation

Campaign name	Time	Number of profiles in the campaign
INTEX-A	In the summer of 2004	105
INTEX-B	In the spring of 2006	115
START08	1 April–16 May and 16–28 June, 2008	60
ARCTAS	March, April, June, and July, 2008	94
HIPPO-1	January, 2009	142
HIPPO-2	October and December, 2009	129
HIPPO-3	March and April, 2010	119

V5 products for ARCTAS, which may be due to the limit of high latitude sample profiles used in the training process, especially north to 75°N and south to 75°S. In these seven campaigns, the RMSEs of the EOF method are mostly less than 2 % in levels under 300 hPa, except for INTEX-A, in which both AIRS-V5 and EOF retrievals have a large overestimation of CH_4. The RMSE of CH_4 retrieved from EOF method is slightly smaller than AIRS-V5, and the RMSE of the EOF method is about 1.5 % in the layer between 359 and 778 hPa. The EOF method cannot provide the information of averaging kernels, and therefore the averaging kernels are not used in the above comparison, which leads to the RMSE for AIRS-V5 a little larger than that obtained by Xiong et al. [25, 26]. We found that the RMSEs above 300 hPa are relatively larger and the correlative coefficients are smaller than the lower layers for both methods, which might be related to the less information content of AIRS and fewer samples used at higher altitudes.

To explore the difference of the retrieval errors from different campaigns and latitudes, the CH_4 in three coarse layers: 359–460, 460–596, and 596–853 hPa were compared. The retrieved CH_4 in these coarse layers were computed as the pressure weighted average using the

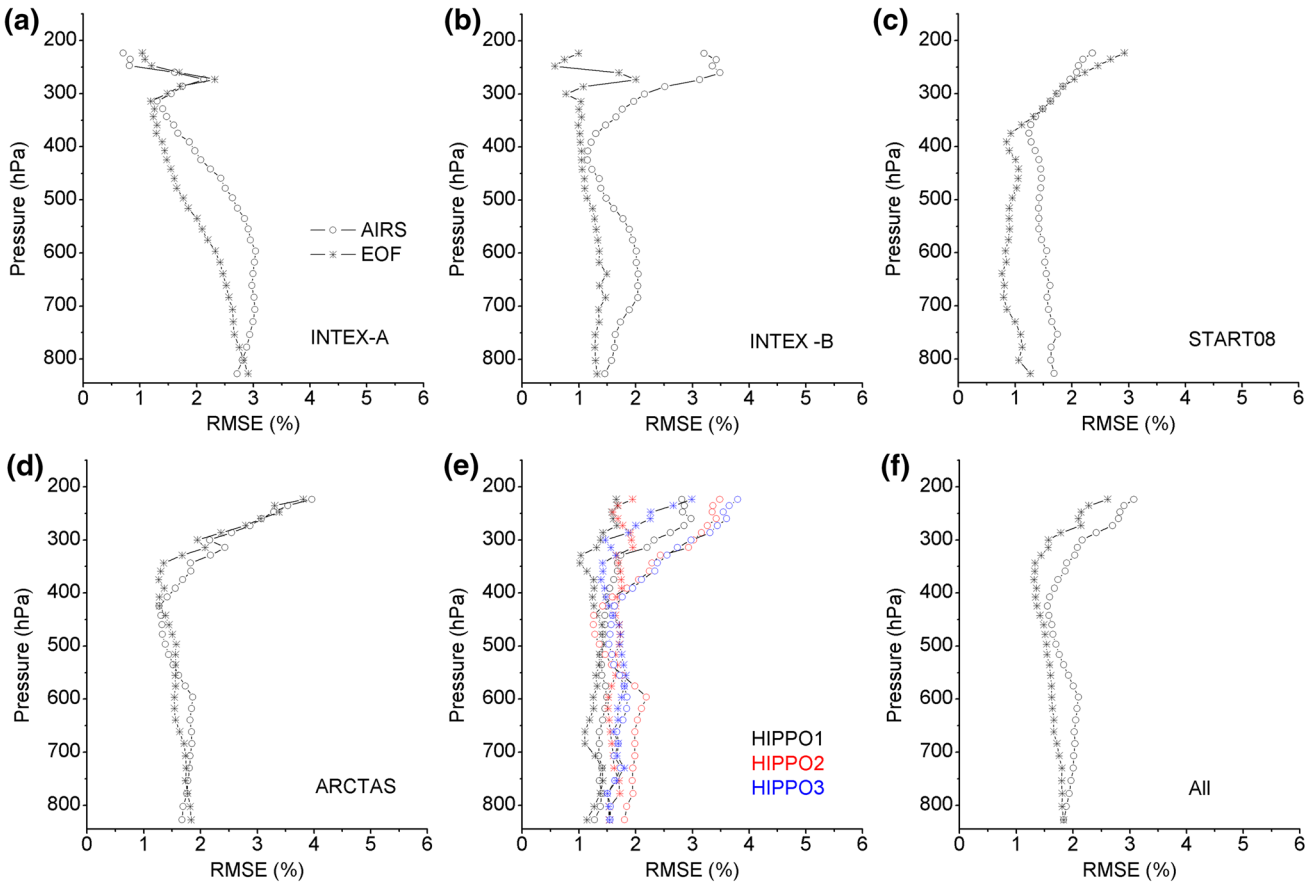

Fig. 5 Similar to Fig. 4 but for the RMSE of CH_4 retrievals

retrievals in the fine 100 layers, and the aircraft measurements were computed similarly. The biases of AIRS-V5 in 359–469 hPa are mostly negative for all the campaigns, while the biases in other two coarse layers are close to zero or positive (Fig. 6a), which may be due to the over-tuning of 2 % to the peak CH_4 channels in AIRS-V5 [25]. This over-tuning has more impact in the tropics, and the error for AIRS-V5 in the high latitude regions can be related to the relatively larger error in temperature and water vapor profiles. For CH_4 retrieved from the EOF method, the biases are mostly negative, except for INTEX-A, -B (Fig. 6a) in 20°–50°N (Fig. 7a), and the large bias in the high latitude regions is likely due to fewer samples in the training process, as stated before (Fig. 7b). Overall, the RMSE of CH_4 retrieved from the EOF method is relatively smaller than that of AIRS-V5 CH_4 products without applying the averaging kernels (Fig. 6b), and we also noticed that the AIRS-V5 CH_4 has a larger variation than the EOF regression method, indicating that the EOF regression method is more stable.

3.2 Comparisons of CH_4 total column amount with ground-based FTS measurements

Ground-based solar FTS sites operated within the NDSC (Network for the Detection of Stratospheric Change) provide measurements of the total column amount of CH_4, with three sites in the Southern Hemisphere and 7 sites in the Northern Hemisphere (http://www.ndsc.ncep.noaa.gov/). These ground-based total column measurements provide valuable data for the validation of satellite missions for greenhouse gases measurements [40]. A summary of the locations (latitude, longitude) and elevations for the ten sites is listed in Table 3. Among these 10 sites, IZTC has the biggest error. In site IZTC, the CH_4 total column amount retrieved from the ground-based FTS measurements is in a range of 2.72×10^{19}–2.91×10^{19} molecules cm^{-2}. However, the CH_4 total column amount retrieved from AIRS-V5 or the EOF method is in a range of 3.0×10^{19}–3.4×10^{19} molecules cm^{-2}. Since this site is located on an island with complicated

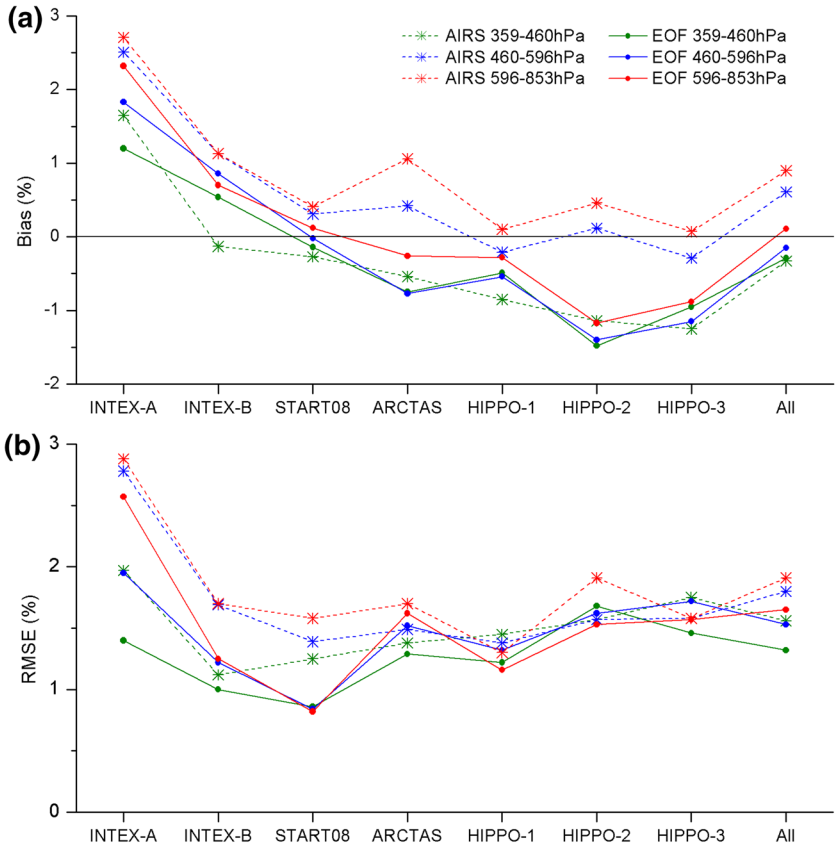

Fig. 6 The mean biases (**a**) and RMSEs (**b**) of CH_4 retrievals for seven campaigns in three coarse layers

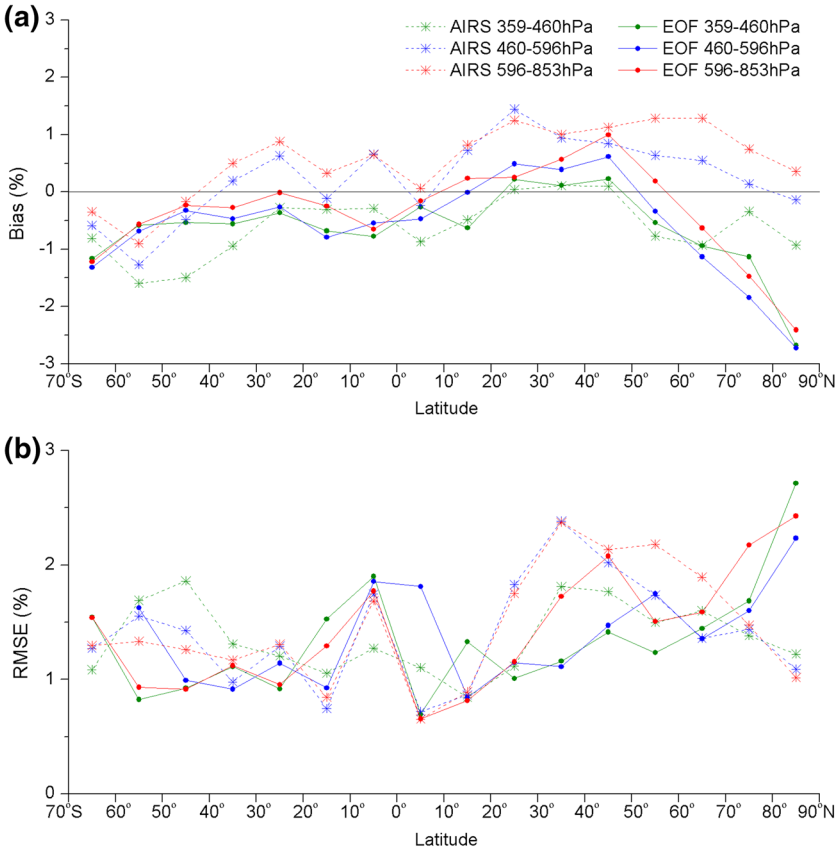

Fig. 7 The mean biases (**a**) and RMSEs (**b**) of CH_4 retrievals in three coarse layers and different latitudes

Table 3 A brief description of the ground-based FTS stations

Site	Sites	Latitude	Longitude	Altitude (km)	Description	Time
ARTC	Arrival HGTSTOTALCOL Antarctica	77.825°S	166.65°E	0.020	Bruker IFS 120M	2002-09 to 2009-12
BMTC	Bremen, Germany	53.107°N	8.854°E	0.027	Bruker IFS125HR	2002-09 to 2007-12
		53.104°N	8.850°E			2008-01 to 2011-08
HRTC	Harestua, Norway	60.2°N	10.8°E	0.596	Bruker IFS 120M	2002-09 to 2010-12
IZTC	Izana, Tenerife, Spain	28.3°N	16.48°W	2.367	Bruker 120M	2002-09 to 2007-12
KRTC	Kiruna Sweden	67.84°N	20.41°E	0.419	Bruker 120HR	2002-09 to 2007-11
LATC	Lauder, New Zealand	45.038°S	169.684°E	0.037	Bruker 120HR	2002-09 to 2009-12
NYTC	Ny-Aalesund Spitsbergen	78.92°N	11.92°E	0.02	Bruker IFS120HR	2002-09 to 2009-08
THTC	Thule, Greenland	76.52°N	68.76°W	0.225	Bruker 120 M	2002-09 to 2007-10
TOTC	Toronto, Canada	43.66°N	79.4°W	0.174	Bomem DA-8 Fourier Transform Infrared	2002-09 to 2009-12
WOTC	Wollongong, Australia	34.453°S	150.883°N	0.03	Bomem DA-8 Fourier Transform Infrared	2003-01 to 2004-12
		34.406°S	150.879°N			2005-01 to 2008-12

geomorphological ground surface, it will not be used in the next discussion.

From the other nine sites, a total of 2,893 observations were used for comparison. Similar to the profile validation, AIRS retrievals within 200 km over the FTS site were used, and their mean was compared with the daily average of CH_4 total column amount from FTS measurements. Data of the AIRS-V5 CH_4 total column amount are from AIRS Level-2 Version 5 Standard Products. The CH_4 total column amount for the EOF method was computed using the surface

pressure and water vapor from AIRS Level-2 Version 5 support products together with the CH_4 mixing ratio profile from the EOF method. A summary of the validation results is listed in Table 4. Comparison of the CH_4 total column amount from AIRS-V5 and the EOF method (Table 4; Fig. 8) shows that the CH_4 total column amount from AIRS-V5 is mostly overestimated (except WOTC) and has a larger RMSE than the EOF method, which agrees with the fact that the CH_4 mixing ratio from AIRS-V5 has a positive bias under 460 hPa. Additionally, the CH_4 retrieval from EOF method has a better correlation with ground-based FTS measurements than AIRS-V5 when all data are combined together. From the histogram of the relative error (Fig. 9), it is evident that the errors of EOF method are mostly in a narrow range of ±2 %, while the errors of AIRS-V5 are in a broader range of ±4 %. This indicates that the EOF method performs better in the retrieval of CH_4 total column amount than AIRS-V5.

Table 4 Validation results of CH_4 total column amount with ground-based FTS observations

Site	Number	Correlation coefficient		Bias (%)		RMSE (%)	
		AIRS	EOF	AIRS	EOF	AIRS	EOF
ARTC	188	0.1586	0.5863	4.11	−0.48	4.84	1.88
BMTC	337	0.4161	0.2353	2.68	0.13	3.07	1.63
HRTC	270	0.5331	0.4500	5.00	0.75	5.28	1.83
KRTC	267	0.4188	0.4408	3.47	0.76	4.17	2.37
LATC	682	0.5405	0.4153	2.39	−0.47	2.85	1.64
NYTC	148	0.1088	0.2434	3.51	0.71	4.40	2.42
THTC	144	−0.0995	−0.0445	1.83	−0.92	4.03	3.06
TOTC	376	0.0308	−0.0097	2.12	0.33	3.44	2.59
WOTC	481	0.2513	0.1902	−3.42	−1.21	3.99	2.29
All	2893	0.7074	0.8883	1.91	−0.15	3.84	2.12

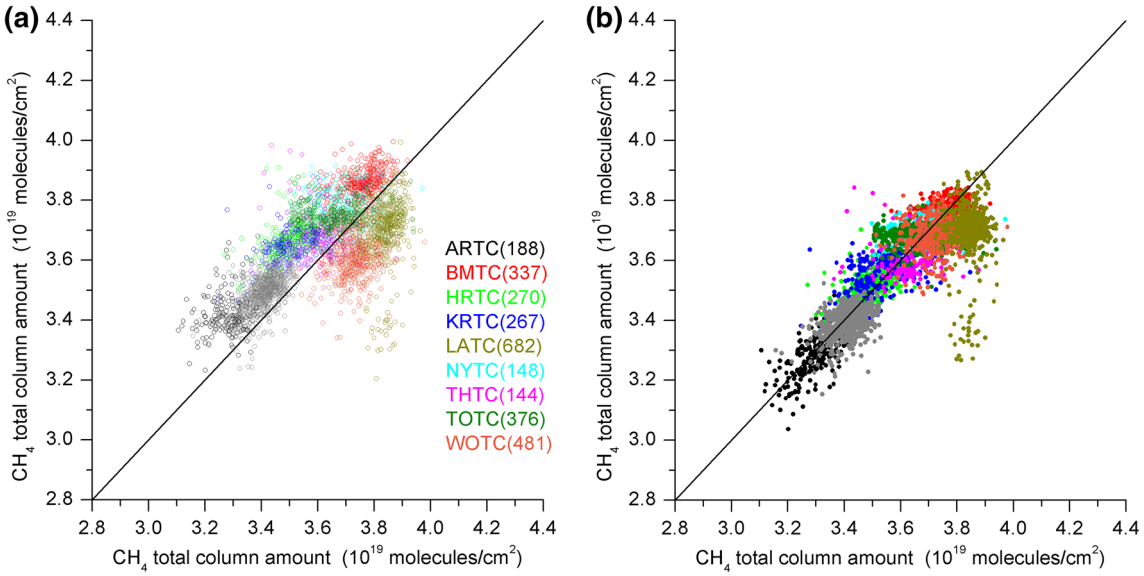

Fig. 8 (Color online) Scatter plot of AIRS retrievals versus in situ FTS observations of CH_4 total column amount for 9 sites. *X*-axis is the ground-based FTS observations. *Y*-axis is AIRS-V5 CH_4 product for (**a**), and EOF retrievals for (**b**). The *black line* is the 1:1 line. The overall Adj. $\boldsymbol{R}^2$ of AIRS-V5 CH_4 product is 0.500, and that of EOF retrievals is 0.789. The mean bias of AIRS-V5 CH_4 product is 1.91 % (RMSE 3.84 %), and that of EOF retrievals is −0.15 % (RMSE 2.12 %)

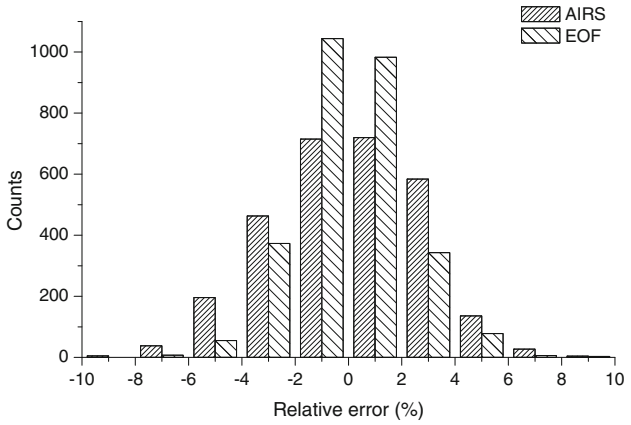

Fig. 9 The histogram of relative errors of CH_4 total column amount (%). The *dense slash bars* are AIRS-V5 CH_4 product, and the *sparse slash bars* are EOF retrievals

4 Conclusions

As a thermal infrared sounder, AIRS on EOS/Aqua platform has provided a unique measurement of mid-upper tropospheric CH_4 since September 2002 and the data have been generated using a physical retrieval algorithm at NOAA and NASA [25]. An improved EOF-based regression retrieval method was introduced and validated in this paper, and this method was developed based on the simulated data and then implemented to derive the CH_4 profiles from AIRS observation. The AIRS 7.7 μm CH_4 band with 50 eigenvectors in the CH_4 profile space and 40 eigenvector in the radiance space are good to be used in the retrieval.

Compared to the physical retrieval algorithm, this regression method is more rapid, stable, and does not rely on the previous knowledge of temperature and water vapor profiles and the CH_4 first-guess profile. Another advantage of this method is its insensitivity to water vapor, which avoids the challenging separation of water vapor, a main interference gas, in the 7.7 μm CH_4 absorption bands. One disadvantage in the EOF method is that it cannot calculate the averaging kernels as in other traditional physical methods, and cannot provide an estimate of the retrieval error either. However, validations using aircraft measurements of profiles show that the correlation coefficients of CH_4 retrieved from the EOF method and AIRS-V5 are almost the same, and the RMSE from the EOF method is slightly smaller. For the layer at 359–460 hPa, the RMSEs of EOF CH_4 are in a range of 1.19 %–1.51 %, and the biases are in a range from −0.75 % to 0.67 %. More validations of the retrieved total column amount of CH_4 with ground-based FTS measurements indicate that the mean bias and RMSE of the CH_4 total column amount from this method are −0.15 % and 2.12 %, both of which are smaller than those from AIRS-V5 CH_4 product. Further comparison with AIRS-V6 will be made in the near future.

The accuracy of the EOF-based regression algorithm is subjected to the representativeness of training data and the error of fast radiative transfer model. This might be the main reason for a worse retrieval from this EOF-based regression method in the campaign ARCTAS. As the input of this retrieval is the cloud-cleared radiance, its error will significantly impact the results. The correlation between two adjacent channels for hyper spectral data also induces redundant information to reduce the accuracy of the model. More improvements might be able to make by incorporating more profiles from the polar region in the training set. Further investigation of these errors and the possibility to train this algorithm using the real observation of radiance and the collocated aircraft measurements of CH_4 profiles from these campaigns will be conducted.

The similar regression retrieval algorithm based on EOF can be easily developed to retrieve CH_4 for other TIR sensors, such as IASI and the Cross-track Infrared Sounder (CrIS), as well as the retrieval of other gases using these TIR sensors. The retrieved CH_4 and other trace gases profiles can, at least, serve as a first guess for further physical retrieval.

Acknowledgments This work was supported by the Strategic Priority Research Program – Climate Change: Carbon Budget and Relevant Issues of the Chinese Academy of Sciences (XDA05090101) and the Institute of Remote Sensing and Digital Earth, Chinese Academy of Sciences (Y1S02000CX). The authors gratefully thank Network for the Detection of Stratospheric Change to provide ground-based FTS measurements. The data of INTEX-A and B used in this publication were obtained from Aura Validation Data Center (AVDC) (http://avdc.gsfc.nasa.gov/index.php) and the aircraft measurements of INTEX-A were carried out by Donald R. Blake of Department of Chemistry, University of California, Irvine; and airborne CH_4 data from INTEX-B and ARCTAS were provided by Glen Sachse and Glenn Diskin of NASA Langley. ARCTAS data were downloaded from (http://ftp-air.larc.nasa.gov/pub/ARCTAS/). The CH_4 data of START08 aircraft measurements were carried out by Dale Hurst and Jim Elkins of NOAA/ESRL/GMD. The CH_4 data of HIPPO aircraft measurements were carried out by S.C. Wofsy, HIPPO science team and cooperating modelers and satellite team.

References

1. Intergovernmental Panel on Climate Change (IPCC) (2007) Climate change 2007: the physical science basis. Cambridge University Press, New York
2. Wuebbles DJ, Hayhoe K (2002) Atmospheric methane and global change. Earth-Sci Rev 57:117–210
3. Etheridge DM, Steele LP, Francey RJ et al (1998) Atmospheric methane between 1000 A.D. and present: evidence of anthropogenic emissions and climatic variability. J Geophys Res 103:15979–15993
4. Schuur EG, Abbott B (2011) Climate change: high risk of permafrost thaw. Nature 480:32–33

5. Dlugokencky EJ, Nisbet EG, Fisher R et al (2011) Global atmospheric methane: budget, changes and dangers. Philos Trans R Soc A 369:2058–2072
6. Koven CD, Ringeval B, Friedlingstein P et al (2011) Permafrost carbon-climate feedbacks accelerate global warming. Proc Natl Acad Sci USA 108:14769–14774
7. Dlugokencky EJ, Bruhwiler L, White JC et al (2009) Observational constraints on recent increases in the atmospheric CH_4 burden. Geophys Res Lett 36:L18803
8. Sussmann R, Forster F, Rettinger M et al (2012) Renewed methane increase for 5 years (2007–2011) observed by solar FTIR spectrometry. Atmos Chem Phys 12:4885–4891
9. Hein R, Crutzen PJ, Heimann M (1997) An inverse modeling approach to investigate the global atmospheric methane cycle. Glob Biogeochem Cycles 11:43–76
10. Zhuang Q, Melack JM, Zimov S et al (2009) Global methane emissions from wetlands, rice paddies, and lakes. Eos AGU 90:37–38
11. Villani MG, Bergamaschi P, Krol M et al (2010) Inverse modeling of European CH_4 emissions: sensitivity to the observational network. Atmos Chem Phys 10:1249–1267
12. Houweling S, Hartmann W, Aben I et al (2005) Evidence of systematic errors in SCIAMACHY-observed CO_2 due to aerosols. Atmos Chem Phys 5:3003–3013
13. Frankenberg C, Aben I, Bergamaschi P et al (2011) Global column-averaged methane mixing ratios from 2003 to 2009 as derived from SCIAMACHY: trends and variability. J Geophys Res 116:D04302
14. Saitoh N, Hayashida S, Imasu R et al (2012) Comparisons between XCH_4 from GOSAT shortwave and thermal infrared spectra and aircraft CH_4 measurements over Guam. Sci Online Lett Atmos 8:145–149
15. Morino I, Uchino O, Inoue M et al (2011) Preliminary validation of column-averaged volume mixing ratios of carbon dioxide and methane retrieved from GOSAT short-wavelength infrared spectra. Atmos Meas Tech 4:1061–1076
16. Schneising O, Buchwitz M, Burrows JP et al (2009) Three years of greenhouse gas column-averaged dry air mole fractions retrieved from satellite. Part 2: Methane. Atmos Chem Phys 9:443–465
17. Meirink JF, Eskes HJ, Goede AH (2006) Sensitivity analysis of methane emissions derived from SCIAMACHY observations through inverse modelling. Atmos Chem Phys 6:1275–1292
18. Clerbaux C, Hadji-Lazaro J, Turquety S et al (2003) Trace gas measurements from infrared satellite for chemistry and climate applications. Atmos Chem Phys 3:1495–1508
19. Razavi A, Clerbaux C, Wespes C et al (2009) Characterization of methane retrievals from the IASI space-borne sounder. Atmos Chem Phys 9:7889–7899
20. Kulawik SS, Worden J, Eldering A et al (2006) Implementation of cloud retrievals for Tropospheric Emission Spectrometer (TES) atmospheric retrievals: part 1. Description and characterization of errors on trace gas retrievals. J Geophys Res 111:1–13
21. Crevoisier C, Nobileau D, Fiore AM et al (2009) Tropospheric methane in the tropics -first year from IASI hyperspectral infrared observations. Atmos Chem Phys 9:6337–6350
22. Wecht KJ, Jacob DJ, Wofsy SC et al (2012) Validation of TES methane with HIPPO aircraft observations: implications for inverse modeling of methane sources. Atmos Chem Phys 12:1823–1832
23. Crevoisier C, Nobileau D, Armante R et al (2013) The 2007–2011 evolution of tropical methane in the mid-troposphere as seen from space by MetOp-A/IASI. Atmos Chem Phys 13:4279–4289
24. Xiong X, Barnet C, Maddy ES et al (2013) Mid-upper tropospheric methane retrieval from IASI and its validation. Atmos Meas Tech 6:2255–2265
25. Xiong X, Barnet C, Maddy ES et al (2008) Characterization and validation of methane products from the Atmospheric Infrared Sounder (AIRS). J Geophys Res 113:1–14
26. Xiong X, Barnet C, Maddy ES et al (2010) Seven years' observation of mid-upper tropospheric methane from Atmospheric Infrared Sounder. Remote Sens 2:2509–2530
27. Xiong X, Barnet C, Maddy ES et al (2013) Detection of methane depletion associated with stratospheric intrusion by Atmospheric Infrared Sounder (AIRS). Geophys Res Lett 40:2455–2459
28. Zhang Y, Chen LF, Tao JH et al (2012) Retrieval of methane profiles from spaceborne hyperspectral infrared observations. J Remote Sens 16:232–247
29. Aumann HH, Chahine MT, Gautier C et al (2003) AIRS/AMSU/HSB on the Aqua Mission: design, science objectives, data products, and processing systems. IEEE Trans Geosci Remote Sens 41:253–264
30. Zhang XY, Bai WG, Zhang P et al (2011) Spatiotemporal variations in mid-upper tropospheric methane over China from satellite observations. Chin Sci Bull 56:3321–3327
31. Xiong X, Houweling S, Wei J et al (2009) Methane plume over south Asia during the monsoon season: satellite observation and model simulation. Atmos Chem Phys 9:783–794
32. Schuck TJ, Brenninkmeijer CM, Baker AK et al (2010) Greenhouse gas relationships in the Indian summer monsoon plume measured by the CARIBIC passenger aircraft. Atmos Chem Phys 10:3965–3984
33. Goldberg MD, Qu Y, McMillin LM et al (2003) AIRS near-real-time products and algorithms in support of operational numerical weather prediction. IEEE Trans Geosci Remote Sens 41:379–389
34. Saunders R, Matricardi M, Geer A (2009) RTTOV9.1 Users Guide. Version 1.5
35. Wofsy SC (2011) HIAPER Pole-to-Pole Observations (HIPPO): fine-grained, global-scale measurements of climatically important atmospheric gases and aerosols. Philos Trans R Soc A 369:2073–2086
36. Singh HB, Brune WH, Crawford JH et al (2006) Overview of the summer 2004 Intercontinental Chemical Transport Experiment-North America (INTEX-A). J Geophys Res 111:D24S01
37. Singh HB, Brune WH, Crawford JH et al (2009) Chemistry and transport of pollution over the Gulf of Mexico and the Pacific: spring 2006 INTEX-B campaign overview and first results. Atmos Chem Phys 9:2301–2318
38. Pan LL, Bowman KP, Atlas EL et al (2010) The stratosphere–troposphere analyses of regional transport 2008 experiment. Bull Am Meteorol Soc 91:327–342
39. Jacob DJ, Crawford JH, Maring H et al (2010) The Arctic Research of the Composition of the Troposphere from Aircraft and Satellites (ARCTAS) mission: design, execution, and first results. Atmos Chem Phys 10:5191–5212
40. Sussmann R, Stremme W, Buchwitz M et al (2005) Validation of ENVISAT/SCIAMACHY columnar methane by solar FTIR spectrometry at the Ground-Truthing Station Zugspitze. Atmos Chem Phys 5:2419–2429